SOFT ROBOTICS
Volume 00, Number 00, 2022

DOI: 10.1089/soro.2021.0199

SoRo
Soft Robotics

Kirigami-Inspired 3D Printable Soft Pneumatic Actuators with Multiple Deformation Modes for Soft Robotic Applications

Jin Guo,[1] Zeyu Li,[1] Jin-Huat Low,[2,3] Qianqian Han,[2,3] Chao-Yu Chen,[2,3] Jun Liu,[4] Zhuangjian Liu,[4] and Chen-Hua Yeow[2,3]

Abstract

Soft robots have received much attention due to their impressive capabilities including high flexibility and inherent safety features for humans or unstructured environments compared with hard-bodied robots. Soft actuators are the crucial components of soft robotic systems. Soft robots require dexterous soft actuators to provide the desired deformation for different soft robotic applications. Most of the existing soft actuators have only one or two deformation modes. In this article, a new soft pneumatic actuator (SPA) is proposed taking inspiration from Kirigami. Kirigami-inspired cuts are applied to the actuator design, which enables the SPA to be equipped with multiple deformation modes. The proposed Kirigami-inspired soft pneumatic actuator (KiriSPA) is capable of producing bending motion, stretching motion, contraction motion, combined motion of bending and stretching, and combined motion of bending and contraction. The KiriSPA can be directly manufactured using 3D printers based on the fused deposition modeling technology. Finite element method is used to analyze and predict the deformation modes of the KiriSPA. We also investigated the step response, creep, hysteresis, actuation speed, stroke, workspace, stiffness, power density, and blocked force of the KiriSPA. Moreover, we demonstrated that KiriSPAs can be combined to expand the capabilities of various soft robotic systems including the soft robotic gripper for delicate object manipulation, the soft planar robotic manipulator for picking objects in the confined environment, the quadrupedal soft crawling robot, and the soft robot with the flipping locomotion.

Keywords: Kirigami-inspired design, 3D printable soft pneumatic actuator, soft robotic gripper, soft robotic manipulator, crawling robot, flipping locomotion

Introduction

Conventional rigid-bodied robots, which are often composed of rigid skeletons, rigid links, rigid joints, and electrical motors, can be superb at performing the tasks where fast movement, high positioning precision, or large output power are especially required. However, these rigid-bodied robots are not safe to interact with humans or working spaces and lack of compliance especially in unstructured environments because of their rigid components and conventional

[1]School of Life Science, Beijing Institute of Technology, Beijing, China.
[2]Department of Biomedical Engineering, College of Design and Engineering, National University of Singapore, Singapore, Singapore.
[3]Advanced Robotics Center, College of Design and Engineering, National University of Singapore, Singapore, Singapore.
[4]Institute of High Performance Computing, A*STAR Research Entities, Singapore, Singapore.

actuation mechanisms. Soft robots, made of intrinsically compliant or soft materials, are capable of providing high flexibility and safety features, thereby bridging the gaps between machines, humans, and unstructured environments.[1–4] Thus, soft robotic systems have been applied to diverse fields, ranging from rescue and search robots,[5,6] surgical tools,[7,8] wearable devices for rehabilitation or assistance,[9,10] bioinspired or biomimetic robots,[11,12] and grippers for manipulating fragile objects.[13,14]

Soft actuators play an important role in soft robotic systems and structures. They are used to induce deformation, operation, or locomotion, and can be powered by various methods including chemical reactions,[15] electromagnetic/magnetic mechanism,[16] cable-driven mechanism,[17] smart materials,[12] and pressurized fluids.[18] Among these actuation methods, soft pneumatic actuators (SPAs) have attracted much attention due to a high power-to-weight ratio, safety of operation, and low cost.[9] Ranzani *et al.*[19] proposed a modular SPA for minimally invasive surgery, in which three equally spaced chambers were positioned in a radial arrangement. The extension or bending motions of the actuator can be generated by combining the inflation of these three chambers. Connolly *et al.*[20,21] presented a class of fiber-reinforced soft actuators. The deformation behaviors of these soft fluid actuators depended on the configuration of the fibers.

Similarly, Sun *et al.*[22] proposed a class of SPAs with diversification of bending modality based on fabric patches. Mosadegh *et al.*[23] proposed the fPN (fast pneu-net) actuator for rapidly actuating. It involved an extensible top layer and an inextensible bottom layer reinforced with an embedded paper. The top layer was elongated by inflation and the bottom layer was constrained, thereby resulting in the bending motion. Yap *et al.*[24] developed the bellows-type SPAs that had a similar design with fPN. The bellows-type actuators, fabricated based on the fused deposition modeling (FDM) technology, can be redesigned with two air channels (ACs) for achieving bidirectional bending motions. McKibben-type pneumatic artificial muscle actuator,[25] which is one of the most widely used SPA, was able to induce linear contraction upon air pressurization.

Gorissen *et al.*[26] proposed a balloon-type pneumatic actuator based on the working principle of asymmetric deflection of two polydimethylsiloxane layers, which can produce bidirectional bending motions. Martinez *et al.*[27] presented a class of SPAs that combined a highly stretchable silicone elastomer with inextensible but bendable patterned papers. Different paper configurations during fabrication procedures can induce a wide range of motions. In addition to these soft actuators powered by positive pressure, there are groups of SPAs that use vacuum actuation for soft robotic applications. Tawk *et al.* proposed the bioinspired bending soft vacuum actuators[28] and linear soft vacuum actuators[29] using an FDM 3D printer for soft robotic systems. Jiao *et al.*[30] designed the vacuum-powered twisting SPA to enhance the capabilities of soft vacuum actuators, which can be combined for various soft robotic applications.

Yang *et al.*[31] proposed the muscle-inspired SPAs that were actuated by vacuum. The actuators can generate the linear motion resembling the motion of the linear actuators used in rigid robots. In addition to elastomeric pneumatic actuators, the thin film-based soft inflatable actuators also provide a promising way to actuate soft robots. Such actuators are commonly composed of a series of pouch-like structured units.[32,33] The pouch-like structured unit consists of a single chamber of air and two walls. The two thin walls are bonded together through a heat-sealing process. The thin film-based SPAs with the extension and contraction capabilities are composed of multiple pouch-like structured units stacked on top of each other. The stretching and contracting motions are produced depending on the inflation and deflation of the pouch-like units. The bending motion of film-based SPAs has been achieved through anisotropic expansion using materials with different extensibilities.[34]

In addition, folds have been used to generate anisotropic expansion of the structure for obtaining the bending deformation.[35] Another approach to achieve bending motion has been to use the lateral expansion of parallel pouches upon pressurization.[36] Moreover, the repeated patterns of pouch-like units with constraints that interact with each other were proposed to produce large bending deformations.[37] Three thin film-based SPAs with extension and contraction capabilities were commonly positioned in a radial arrangement to achieve multiple degrees-of-freedom (DoFs) actuation.[32,38] Most of the existing SPAs are with one or two deformation modes. Even though several existing SPAs can be programmed to achieve a wide range of complex motions before fabrication, such as fiber-reinforced soft actuators and some other soft actuators based on the similar working principles, they can only generate one or two motion modes once fabricated.

Kirigami, the ancient Japanese art of paper cutting, has become a promising strategy to achieve highly stretchable devices and morphable structures through designed cuts. Kirigami-inspired structures have been applied to various functional systems such as stretchable electronics,[39] bioinspired robotics,[40] smart sensors,[41] reconfigurable metamaterials,[42] and graphene-based applications.[43] In this article, inspired by the concept of Kirigami, we proposed a new SPA design that was capable of providing multiple deformation modes, including bidirectional bending, extension, contraction, a combination of bending and extension, and a combination of bending and contraction, for expanding the capabilities of soft robotic systems or structures upon pressurization. The Kirigami-inspired soft pneumatic actuator (KiriSPA) was directly fabricated based on the FDM-based 3D printing technique, thereby avoiding the complex multistep processes in the other fabrication methods. Finite element method (FEM) models were built to analyze and predict the deformation modes under different air pressures.

The performance of the KiriSPA was characterized including the step response, creep, hysteresis, and blocked force measurement. From the experimental results, we demonstrated that the addition of Kirigami-inspired cuts enabled the soft actuator to generate various complex motions upon pressurization. In addition, we demonstrated the KiriSPA potential in expanding the functionalities of various soft robotic applications including soft robotic grippers, the soft planar robotic manipulators, the quadrupedal soft crawling robots, and soft flipping robots.

Materials and Methods

Design and working principle of the KiriSPA

The patterned Kirigami cuts can make a variety of deformation behaviors possible. As illustrated in Figure 1a, three

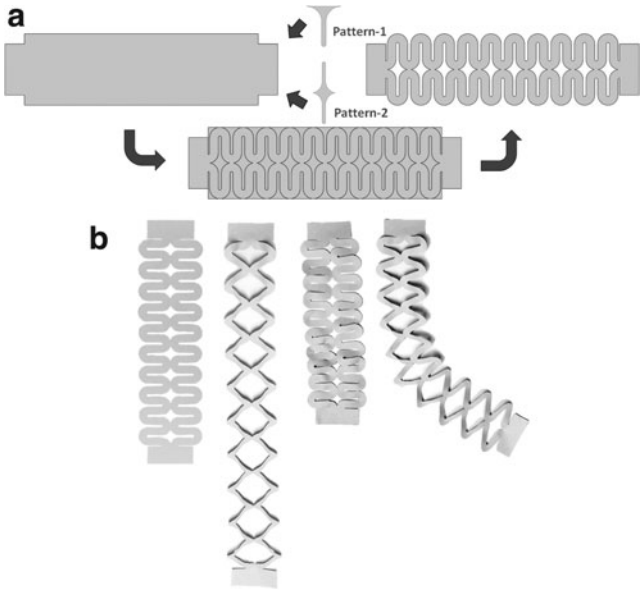

FIG. 1. Schematic illustration of the patterned Kirigami cuts: **(a)** the Kirigami cuts with two different patterns and **(b)** the paper model with the designed Kirigami cuts generating a variety of deformation behaviors.

rows of Kirigami cuts with two different patterns (Pattern-1 and Pattern-2) were designed and applied to a colored paper validating whether this Kirigami structure can enable the paper to achieve multiple deformation modes or not. Pattern-1 was distributed on two edges of the paper, and Pattern-2 was positioned in the center part. As illustrated in Figure 1b, the paper model can be easily in-plane stretched, bent, and contracted, and then it can recover to its original state when without loading, while it is very difficult for the intact paper without Kirigami patterning to be in-plane stretched or bent.

The same Kirigami patterns were applied to the soft actuator design and two corresponding ACs were designed to actuate the Kirigami structure. The geometric parameters for the cuts are illustrated in Figure 2. The same cuts were repeated 10 times along the stretching direction shifted by 12 mm. The cylindrical pneumatic channel in the inlet part was designed to connect ACs to the air source. Obviously, the design of the KiriSPA can be easily scaled down or up to suit different applications.

The actuation principle of the KiriSPA depends on the strain asymmetry when air pressure was supplied. The KiriSPA contains two layers and each layer possesses an AC. The KiriSPA can be actuated by both positive and negative air pressures. When air pressure is supplied to one AC and the other AC is kept at atmospheric pressure, the activated layer induces expanding or contracting strain, while the passive layer working as the constraint layer converts the activated layer's axial deformation to bending motion. When the same air pressure is supplied to both the ACs, two layers induce the same expanding or contracting strain, which can generate the extension and contraction motions based on the Kirigami-inspired structure. When differential positive air pressures are supplied to the two independent ACs, two layers induce differential expanding strains, which can generate the bend/extension coupled motion.

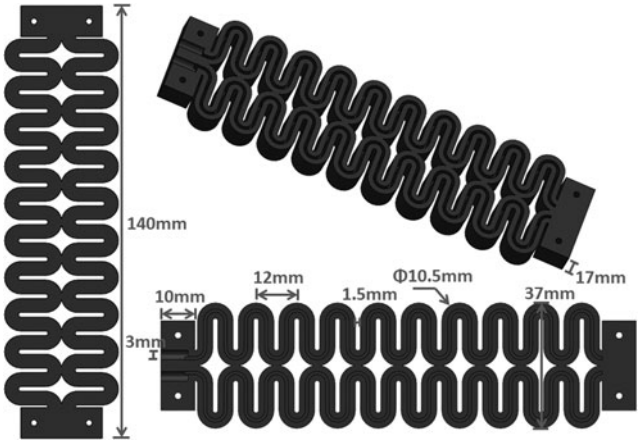

FIG. 2. The design and dimension of the KiriSPA. KiriSPA, Kirigami-inspired soft pneumatic actuator.

Similarly, the KiriSPA can generate the bend/contraction coupled motion when differential negative air pressures are supplied. Thus, the KiriSPA has two DoFs, including one translational DoF and one rotational DoF. Moreover, it is able to produce multiple deformation modes including bidirectional bending, extension, contraction, bend/extension coupled motion, and bend/contraction coupled motion. The input differential pressure can be infinite. Theoretically, the KiriSPA is capable of generating an infinite number of bending motion modes.

Figure 3a presents the bending procedures when positive air pressure (ranging from 0 to 150 kPa with the incremental step of 30 kPa) was supplied to AC-1 and the internal pressure of AC-2 was atmospheric pressure. As illustrated in Figure 3b, the KiriSPA was able to achieve almost 200% stretching displacement at the pressure of 120 kPa, thanks to the Kirigami-inspired structure. Figure 3c and d illustrated the deformation procedures of the bend/extension coupled motion when differential positive pressures (AC-1 was pressurized at 40 kPa and AC-2 was pressurized from 40 to 190 kPa with the incremental step of 30 kPa, AC-1 was pressurized at 60 kPa and AC-2 was pressurized from 90 to 190 kPa with the incremental step of 20 kPa) were supplied. Figure 3e presented the bending motion generated when positive and negative air pressures were simultaneously supplied to AC-1 and AC-2, respectively.

This configuration was capable of achieving full bending at the pressure of 120 kPa, which was lower than the pressure value used in Figure 3a. In addition, the radius of the actuator during the bending motion was also smaller than that during the bending motion generated by only positive pressure. Figure 3f showed the bending motion induced when the negative pressures of −10 and −90 kPa were supplied to AC-2, respectively. Figure 3g illustrated the contraction procedures when the equal negative air pressures of −10 and −90 kPa were simultaneously supplied to AC-1 and AC-2, respectively. The KiriSPA shrunk to its compact state with Kirigami cuts closed. A video of the KiriSPA generating multiple deformation behaviors is available as Supplementary Movie S1.

Finite element analysis

Finite element analysis was conducted to prove the feasibility of the Kirigami design and understand the mechanics of

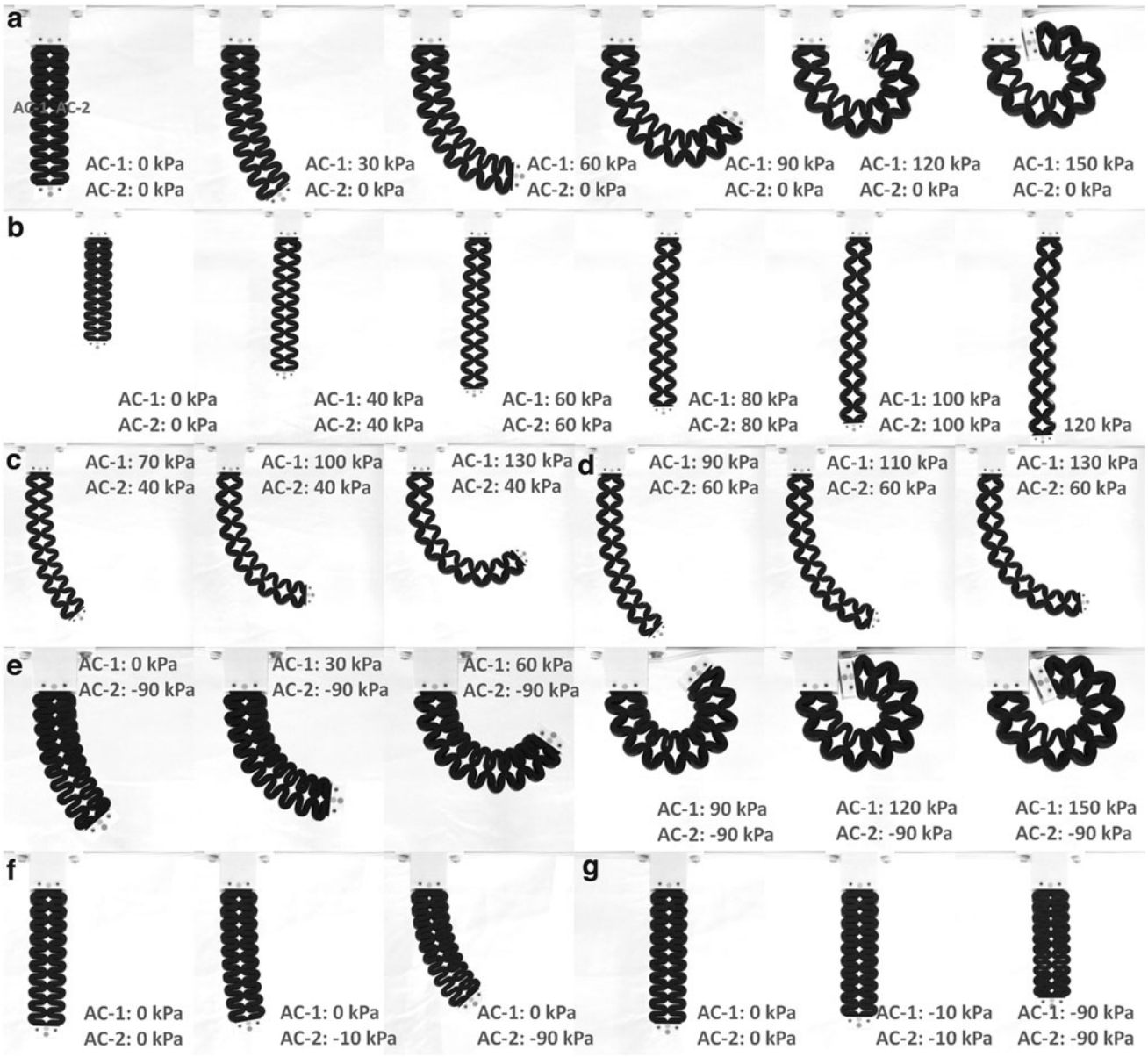

FIG. 3. The deformation behaviors of the KiriSPA: **(a)** bending when positive air pressure was supplied; **(b)** stretching; **(c, d)** bending/stretching coupled deformation; **(e)** bending when negative air pressure was supplied; **(f)** contraction; and **(g)** bending/contraction coupled deformation when positive and negative air pressures were simultaneously supplied.

the deformation behaviors. The deformation behaviors of the KiriSPA under different input air pressures obtained using finite element analysis are illustrated in Supplementary Data and Supplementary Figure S1.

Fabrication of the KiriSPA

The KiriSPA was directly fabricated using the FDM-based 3D printing technique. The fabrication process and optimized printing parameters are described in Supplementary Data.

Results

Characterization of the KiriSPA

To evaluate the performance of the KiriSPA, three circular markers were attached to the ends of the actuator. A blue circular marker, located on the proximal end of the KiriSPA, was used to indicate the original point in the image coordinate. In addition, a red circular marker and a blue circular marker, positioned on the distal end of the actuator, were used to demonstrate the final position and bending angles. An image-processing algorithm to detect and track these three markers was implemented using the image processing toolbox of MATLAB (R2017a; the MathWorks, Inc., Natick, MA).

Step response and actuation speed. The bending, extension, and contraction motions of the KiriSPA were measured based on the movements of the markers extracted from the video frames. The bending angles and linear displacements of the markers upon activation with the input air

pressure of 140, 120, and −90 kPa were calculated to evaluate the step response performance of the actuator. The step response test for each motion was repeated five times. As illustrated in Figure 4a, the actuator showed a rapid response when the pressurized air or vacuum was applied. In addition, the actuator returned to its initial position rapidly when the pressure supply was cut off. Three KiriSPAs were used for the experiments. For the bending motion, the rise time was $\sim 420 \pm 50$ ms that was calculated from the step response data and the decay time was 340 ± 24 ms. The actuation speed of the bending motion was $\sim 0.67°$/ms.

However, the KiriSPA appeared to oscillate after recovering its initial position, and additional time was needed for the actuator to stop the oscillation. In addition, the rise time for stretching and contracting motions was $\sim 1.14 \pm 0.06$ and 0.51 ± 0.1 s, respectively, and the decay time for these two

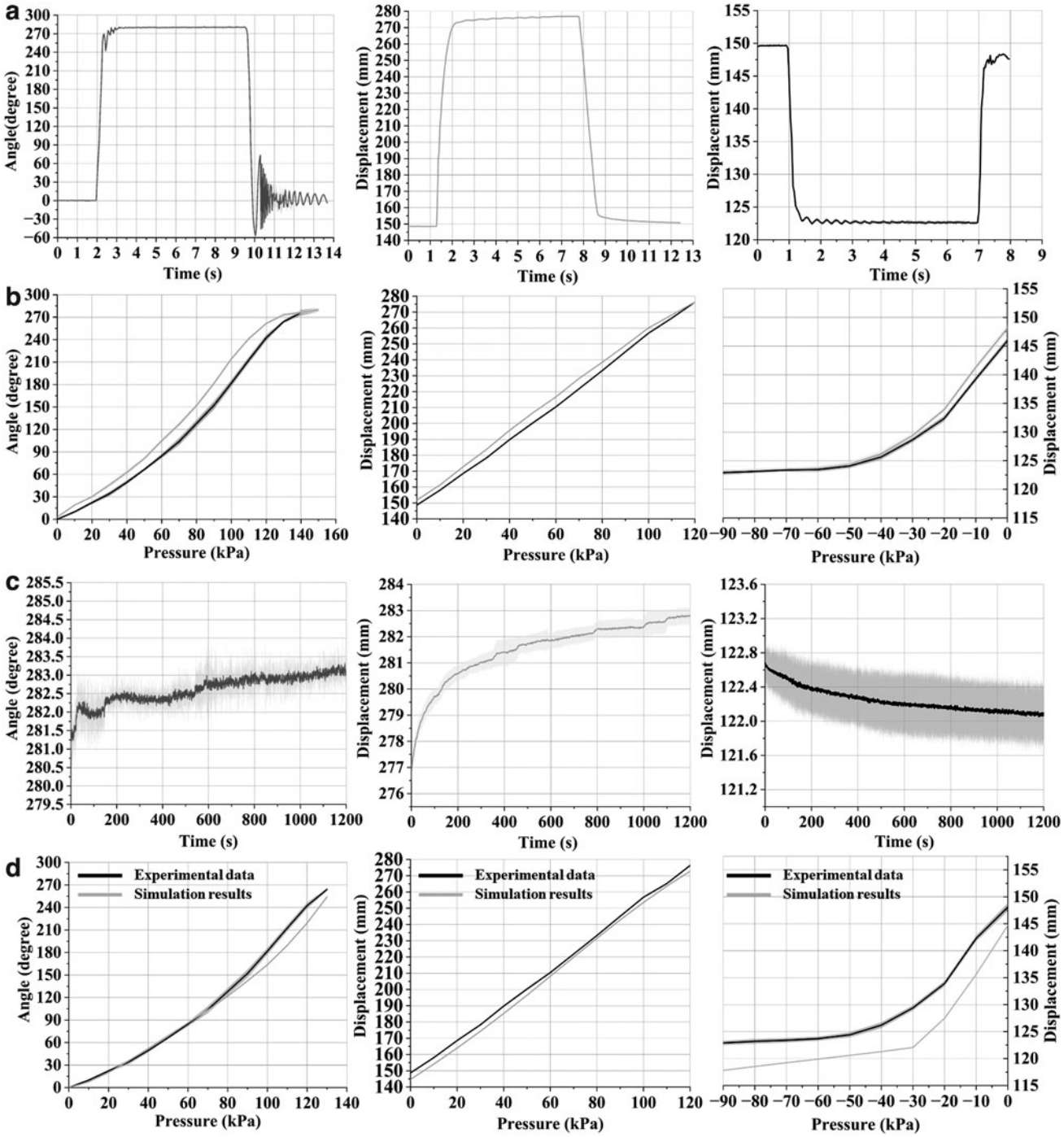

FIG. 4. Step response, creep, and hysteresis characterization of the KiriSPA: **(a)** step response curves; **(b)** creep curves in 20 min; **(c)** hysteresis curves; and **(d)** comparison between the FEM models and the experimental data. (The *columns* in each subfigure: bending motion, stretching motion, and contraction motion.) FEM, finite element method.

motions was 1.08 ± 0.04 and 0.42 ± 0.08 s, respectively. Accordingly, the actuation speed of stretching and contracting motions was ~ 112.9 and 55.2 mm/s, respectively.

Hysteresis. For the bending and stretching motions of the KiriSPA, we monitored the bending angles and linear displacement of the markers attached to the actuator tip when the supplied pressure was ramped up and down from the pressure of 0 kPa by a positive pressure of 10 kPa in each step. In addition, the linear displacement of the KiriSPA was measured when the negative pressure was ramped up and down from the pressure of 0 kPa by a negative pressure of −10 kPa in each step. The hysteresis test for each motion was repeated five times. The experimental results are illustrated in Figure 4b. Three KiriSPAs were tested in the experiments. For these three deformation behaviors, the KiriSPA showed hysteresis with the largest difference of $34.2° \pm 2.4°$, 8.4 ± 2.2, and 1.9 ± 0.42 mm occurring at the pressure of 100, 50, and −10 kPa, respectively.

Creep. Two precision regulators (IR2020-02B-A and IRV20-C06BG; SMC Corporation, Japan) were used to modulate the positive and negative pressure supplied to the actuator, respectively. The actuator was first activated by the positive pressure. The bending motion of the KiriSPA was activated at the pressure of 140 kPa. The supplied pressure remained constant for more than 20 min, while the position of the markers attached to the actuator was monitored to detect any drift from their original position resulting from creep. After that, the KiriSPA was stretched by the supplied pressure of 120 kPa and its actuator tip was monitored in another 20 min. In addition, the KiriSPA was actuated by negative pressure for another 20 min while the tip position of the actuator was also monitored with time. The creep test for each motion was repeated five times.

As shown in Figure 4c, the position of the actuator slightly changed in bending and stretching motions and remained almost unchanged during the vacuum activation period. Three KiriSPAs were tested in the experiments. The bending angles and the stretching displacement increased $2.6° \pm 0.4°$ and 5.4 ± 1.12 mm, respectively. The contracting displacement decreased 0.4 ± 0.2 mm. The cumulative experimental time for one KiriSPA exceeded 5 h. During experiments with positive pressure and negative pressure, the pressure values remained almost unchanged, which demonstrated that the KiriSPA was perfectly fabricated almost without air leakage.

Stroke, workspace, and stiffness. During the stroke characterization tests, the positive pressure was supplied to the KiriSPA with the step of 10 kPa for the bending and stretching motions, and the negative pressure was supplied with the step of −10 kPa for the contracting motion. The bending angles and displacements with respect to the input pressure values were simultaneously recorded. The test for each motion was repeated five times, and the experimental results are illustrated in Figure 4d. The KiriSPA can achieve a bending angle of $281.5° \pm 1.6°$ and a length of 276.3 ± 0.4 mm. We compared the measured bending angles and displacements from the experiments with the values obtained from FEM models. From the experimental results, the deformation behaviors from simulation results had good agreement with the results from experiments.

The FEM models demonstrated the average relative error of 7.7%, 1.6%, and 4.1%, with a maximum relative error of 12.1%, 2.8%, and 6%, for the bending, stretching, and contracting motions, respectively. This is acceptable when estimating the deformation in the phase of structural design.[44] A coordinate system was built to determine the corresponding workspace of the KiriSPA, as illustrated in Supplementary Figure S2a. We chose the origin of the coordinate system at the position of the blue marker attached on the proximal end of the KiriSPA. Another blue marker attached on the actuator tip was tracked by an image-processing algorithm. The KiriSPA first stretched and then swept its reachable workspace using the bend/extension coupled motion. Since the KiriSPA is axisymmetric, the reachable workspace in the first and fourth quadrants was representative of the whole workspace, as illustrated in Supplementary Figure S2b.

The experimental setup to measure the stiffness of the KiriSPA is illustrated in Supplementary Figure S3. The stiffness was defined by using a force that resulted in a displacement. The stiffness of the KiriSPA was measured in both lateral and longitudinal directions. The test for each direction was repeated five times. We used the forces measured at a displacement of 5 mm to describe the actuator stiffness. From the experimental results, the actuator stiffness was 0.03 N/mm (lateral direction) and 0.11 N/mm (longitudinal direction), respectively.

Blocked force measurement and power density. Two force measurement experiments were conducted using a force gauge (SI-65-5, ATI Industrial Automation, Inc.) to measure the blocked force of the actuator in bending, stretching, and contraction motions. In the experiments, the stretching motion, contraction motion, or the bending motion of the actuator was restricted by a mounting fixture and a customized constraining platform. As illustrated in Supplementary Figure S4, the proximal end of the KiriSPA was fixed on the mounting platform and the ACs were connected to the air pressure source. The tip of the KiriSPA was positioned in contact with the force gauge. In the blocked force experiment for bending motion, the constraining platform was positioned on the actuator to restrict the bending curvature of the actuator (shown in Supplementary Fig. S4a), which was similar to measurement setups used in previous studies.[24,45]

This experimental setup allowed the force gauge to measure the maximum tip force generated by the KiriSPA upon air pressurization. In addition, we also measured the force at three bending angles (shown in Supplementary Fig. S4b), including 30°, 60°, and 90°. It is noteworthy that this experimental setup was only capable of measuring the maximum tip force exerted by the actuators at a constant bending curvature with different air pressures. It did not measure the force when the bending angle increased.

The actuator started to deform and trigger the force gauge when the air pressure was supplied. Three KiriSPAs were used for the experiments and the blocked force test for each motion was repeated five times. The force measured in both bending and stretching motions was increased with the increasing input positive air pressure. The maximum force for the bending and stretching motions was 10.6 ± 0.58 N (0°), 10.1 ± 0.45 N (30°), 9.8 ± 0.43 N (60°), 7.9 ± 0.37 N (90°), and 52.3 ± 1.14 N (0°), 45.8 ± 0.89 N (30°), 39.1 ± 0.74 N (60°),

and 32.7 ± 0.71 N (90°). Their corresponding actuation pressures were 260 kPa. For the contracting motion, the maximum force and its corresponding actuation pressure were 3.55 ± 0.24 N and −90 kPa.

Based on the actuation speed and the maximum generated forces, the power densities can be calculated using the method in Rogatinsky *et al*.[32] The results were 113.6 and 3.8 W/kg in the stretching and contracting motions.

Applications of Kirigami-inspired actuators

The proposed KiriSPA is capable of producing multiple deformation behaviors. Two or more KiriSPAs can be combined to expand robots' capabilities in a variety of soft robotic applications such as soft robotic grippers, soft robotic manipulators, and locomotion robots.

Soft robotic grippers. Soft pneumatic bending actuators have been used to form various soft robotic grippers or hands for manipulating delicate objects due to their inherent compliance and air compressibility.[46–52] However, to the best of the authors' knowledge, most researchers focused on the grasping modes of soft robotic grippers, variable stiffness principles, and the sensory feedback systems. Few research achievements on soft robotic grippers with stretchable ''fingers'' have been reported.

The soft robotic gripper composed of KiriSPAs also has the same advantages as the existing soft grippers in safely interacting with objects. A three-finger gripper was fabricated based on three KiriSPAs. We validated the performance of the three-finger soft gripper by gripping different objects with different shapes, sizes, and mechanical properties. It was capable of gripping a strawberry, a green vegetable, a piece of sushi, a piece of broccoli, a piece of bread, a pudding, a wine glass, a plastic box, and a bag of instant noodles, as shown in Figure 5 and Supplementary Movie S2. When gripping the plastic box, the gripper was able to grip it from inside, which was different from the previous gripping tasks. When gripping the object with a larger size than the ''palm'' such as the bag of instant noodles, the gripper was capable of increasing the open width, thereby realizing the gripping of larger objects.

Moreover, the combination of the KiriSPAs was capable of generating new capabilities to enhancing the existing soft gripper properties. A two-finger gripper and a one-finger gripper based on KiriSPAs were fabricated to validate the gripping performance in a confined environment, as shown in Figure 6a. A strawberry was positioned inside two acrylic walls. The distance between the two walls was 35 mm, which was very difficult for the ''palm'' to approach the strawberry. When gripping the strawberry, KiriSPAs were first pressurized to induce the stretching deformation for approaching the strawberry. The combination motion of stretching and bending was then induced to grip the strawberry. The input pressure was not increased once the strawberry is pinched. Thus, the folds did not trap and damage the strawberry.

Finally, the KiriSPAs were depressurized to pick the strawberry out of the confined environment. In addition, we also demonstrated the gripping performance of the one-finger gripper when the strawberry was stuck between two walls. In this case, the KiriSPA was actuated to approach the strawberry and wrapped around it for a stable grasp (shown in

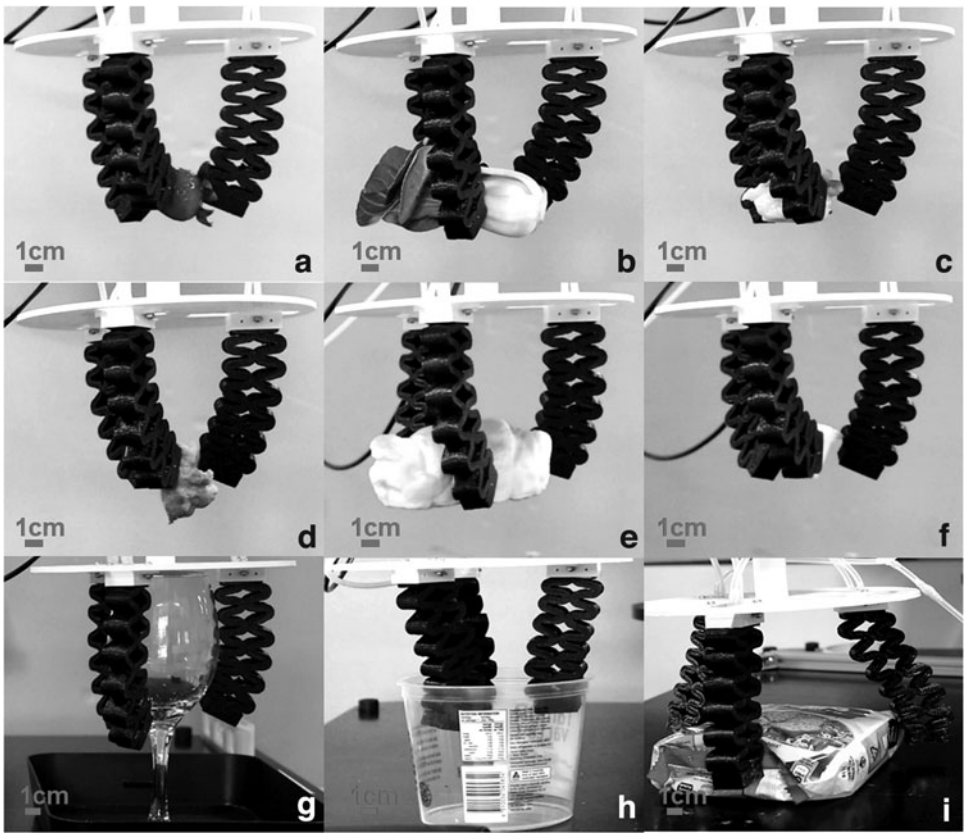

FIG. 5. The three-finger soft robotic gripper for gripping various objects: **(a)** strawberry; **(b)** green vegetable; **(c)** sushi; **(d)** broccoli; **(e)** bread; **(f)** pudding; **(g)** wine glass; **(h)** plastic box; and **(i)** instant noodles.

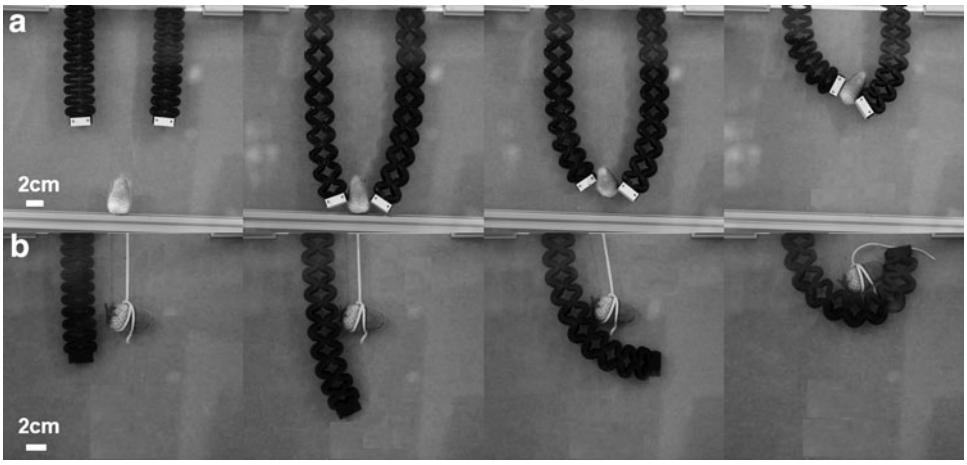

FIG. 6. The soft robotic gripper for gripping the object in the confined environment: **(a)** pinching the strawberry and **(b)** wrapping around the strawberry.

Fig. 6b). The strawberry was positioned on the finger and the folds may not trap and damage the strawberry.

Soft planar robotic manipulator with vacuum suction cup. Soft robotic manipulators are not only with the ability to safely interact with the environment due to their inherent compliance, but are capable of being compliant and possessing more DoFs, which allows them to execute highly dexterous tasks in the confined environment. Three KiriSPAs can be connected in series using two 3D-printed fixture parts to form a soft deformable planar robotic manipulator. Two gripping experiments within a confined environment were conducted to validate the soft planar robotic manipulator's ability to navigate through obstacles.

The primary purpose of these two experiments is to test whether the soft planar robotic manipulator can advance the suction cup to reach various positions through the confined environment for picking objects. A suction cup was attached to the distal part of the manipulator as the end effector for gripping the objects (shown in Supplementary Movie S3). The proximal end of the soft planar robotic manipulator was fixed to an aluminum bar near the entrance of the confined environment. Figure 7 depicts the manipulator advancing from the entrance to the target objects in the confined environment. First, the vacuum suction cup was advanced to reach the neighboring area of the target object by the combined motion of bending and stretching. The internal pressures in both the left and right ACs of the distal KiriSPA were then slightly modulated to make the vacuum suction cup tightly contact the surface of the target object.

It is difficult to realize this function using the existing soft bending actuators because a little air leak will result in failure to gripping the target objects. Fortunately, KiriSPAs are able to provide multiple deformation modes and we can position the suction cup perpendicular to the surface of the target object. The contact force can be generated to push the suction cup to the object's surface, which can significantly improve the success rate of the gripping operations. In addition, it is difficult for the thin film-based SPAs[32,38] to achieve these picking tasks due to their limited initial length and maximum inflated length. Compared with these actuators, the initial length of the beam-shaped KiriSPAs can be customized

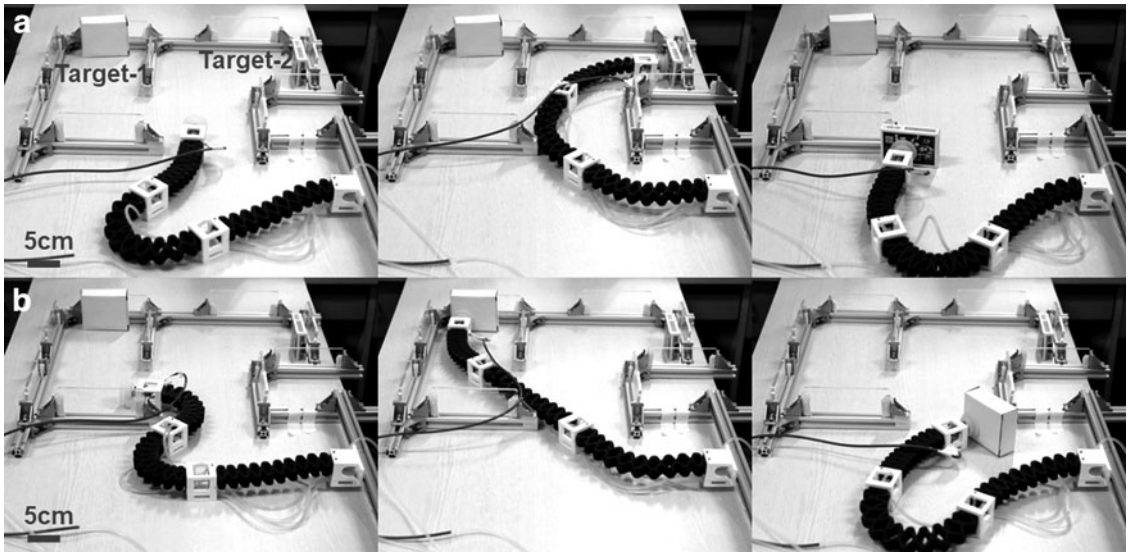

FIG. 7. The soft planar robotic manipulator with vacuum suction cup for picking objects in the confined environment: **(a)** gripping target-1 and **(b)** gripping target-2.

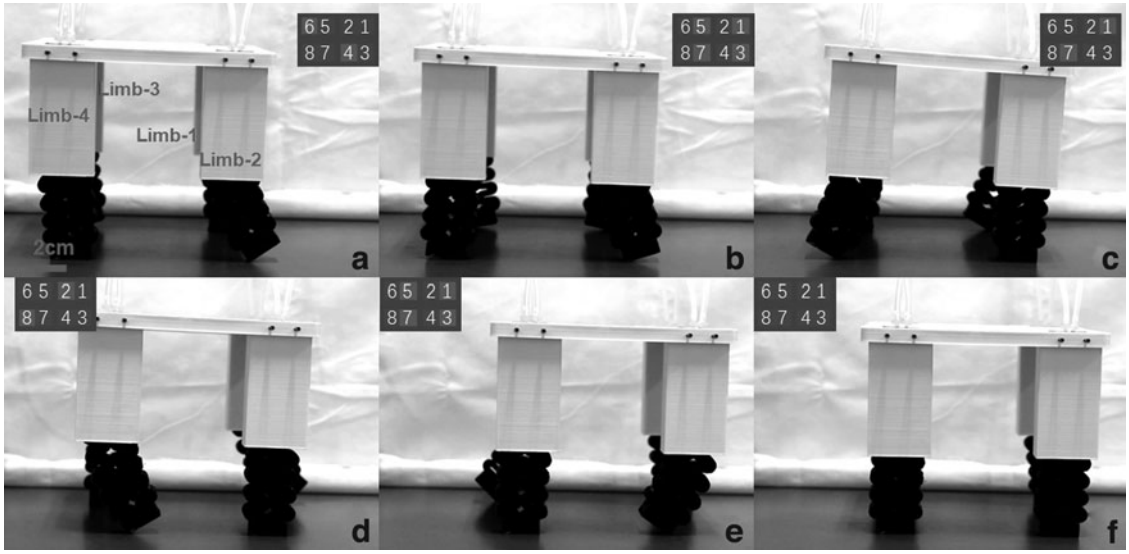

FIG. 8. The walking gait of the quadruped crawling robot: **(a–f)** cycles of pressurization and depressurization of ACs that result in walking locomotion. (The number of ACs highlighted with *orange* represents pressurization, and the number of ACs highlighted with *gray* represents depressurization.) AC, air channel.

according to different applications. Finally, the manipulator was controlled to take the target objects out of the confined environment by reducing the supplied air pressure.

Quadruped crawling robot with stretchable limbs. We designed and fabricated a quadruped crawling robot, combined with four KiriSPAs as limbs, further demonstrating the KiriSPA's advantages. The crawling robot's body was made of 3D-printed acrylonitrile butadiene styrene material. Each AC inside each limb can be independently controlled. Thus, this crawling robot is capable of lifting any one of its four limbs off the ground and leaves the other three legs planted to provide stability. The crawling robot was actuated by pressurizing the limbs in sequence. Figure 8 shows the walking gait of the quadruped robot.

No ACs were pressurized in the initial state of the crawling robot and one actuation sequence consisted of six steps: (i) Sequential pressurization of AC-4 and AC-6, Limb-2 and Limb-3 were successively lifted from the ground and bent forward to contact the ground (Fig. 8a). (ii) Simultaneous pressurization of AC-1, AC-3, AC-5, and AC-7 and depressurization of AC-4 and AC-6 pushed the crawling robot forward with Limb-2 and Limb-3. At this point, the reaction forces generated by the frictional force propelled the robot to move forward while the Limb-1 and Limb-4 were pulled to the bent state (Fig. 8b). (iii) Simultaneous depressurization of AC-3 and AC-5 made the Limb-2 and Limb-3 recover to the straight state (Fig. 8c). (iv) Sequential depressurization of AC-1 and AC-7 and pressurization of AC-2

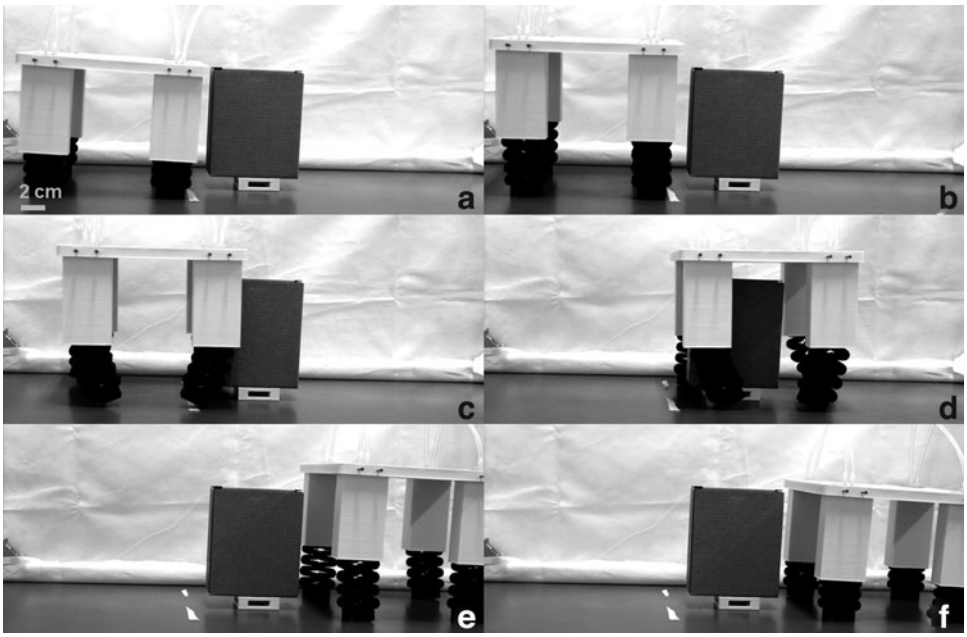

FIG. 9. The quadruped crawling robot moving over an obstacle: **(a–f)** cycles of pressurization and depressurization of ACs that drive the robot walking through the obstacle.

and AC-8, Limb-1 and Limb-4 were successively lifted from the ground and swung from back to front (Fig. 8d).

(v) Simultaneous pressurization of AC-1, AC-3, AC-5, and AC-7 and depressurization of AC-2 and AC-8 pushed the crawling robot forward with Limb-1 and Limb-4 (Fig. 8e). (vi) Sequential depressurization of AC-3, AC-5, AC-1, and AC-7 made the crawling robot recover its initial state (Fig. 8f). The actuation sequence was repeated to generate the crawling locomotion.

To demonstrate the potential of the crawling robot with KiriSPAs to accomplish tasks that would be difficult or impossible with the existing bending SPAs, we drove the robot moving over an obstacle: a box with a similar height to the robot (shown in Fig. 9a). In this condition, the robot cannot directly walk over the obstacle without collision. To overcome the obstacle, four limbs of the crawling robot were stretched by supplying the same initial air pressure before we propelled the robot to the obstacle (shown in Fig. 9b). After that, the height of the crawling robot grew over the obstacle. The actuation sequence mentioned above was then conducted to drive the robot walking through the obstacle (illustrated in Fig. 9c–f). The video of this crawling robot walking over the obstacle is available as Supplementary Movie S4.

Flipping locomotion. The ability to induce bidirectional bending motions and the combined motions of bending and stretching makes the KiriSPA suitable to generate flipping locomotion. The flipping robots consisted of one or two KiriSPAs and two vacuum suction cups (shown in Fig. 10). Two suction cups were used as the grippers and integrated

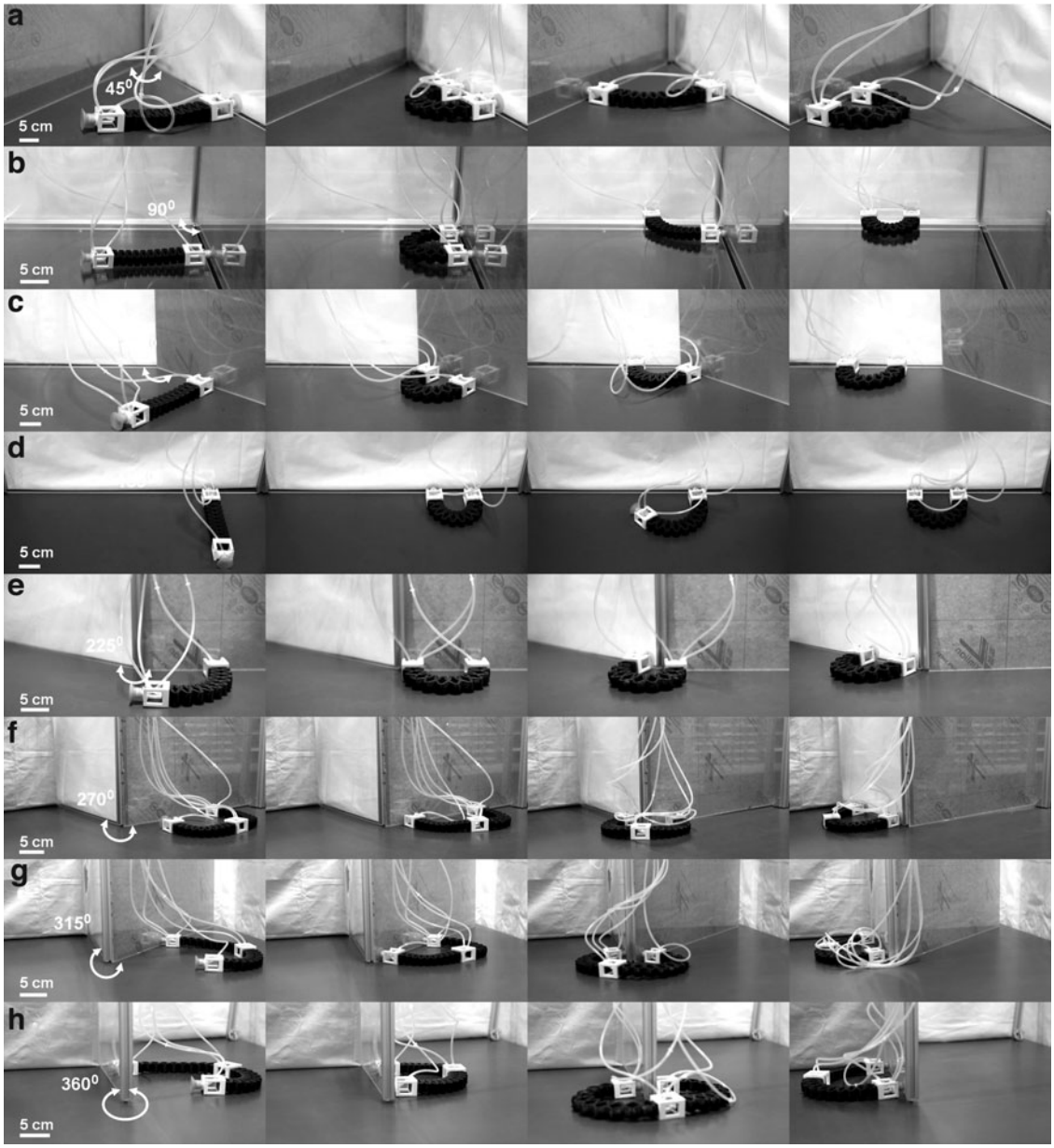

FIG. 10. The soft robot with flipping locomotion based on one or two KiriSPAs for transition between two surfaces: **(a)** 45° ; **(b)** 90°; **(c)** 135°; **(d)** 180°; **(e)** 225°; **(f)** 270°; **(g)** 315°; and **(h)** 360°.

with both ends of the flipping robot. We demonstrated the robots' ability to flip consistently over a flat acrylic surface and transition between surfaces. One suction cup was attached to the wall surface and the other was free in the initial state. Next, the corresponding AC was pressurized to drive the robot flipping to the required direction.

The supplied air pressure values were then slightly modulated to make the free suction cup tightly contact the wall surface. After that, the free suction cup was actuated by supplying the vacuum pressure, which allowed it to firmly grip the wall surface. Then, the other suction cup was released and repositioned for the next flipping gait or to transition between two surfaces. To evaluate the performance of the flipping robots, a series of experiments were conducted to validate the robots' ability to transition between surfaces. Two acrylic walls were positioned with the angles of 45°, 90°, 135°, 180°, 225°, 270°, 315°, and 360°. From the experimental results, the flipping robot with one KiriSPA was capable of transitioning the walls with the angle of 225° to the maximum extent, and the robot with two KiriSPAs was able to transition between the walls with all the intersection angles (shown in Supplementary Movie S5).

Conclusions and Future Work

A new method of designing SPAs based on Kirigami patterning is presented in this article. The Kirigami-inspired design approach has demonstrated its versatility and efficiency in providing various deformation behaviors when air pressures were supplied. Moreover, we demonstrated that two or more KiriSPAs can be combined to potentially expand the capabilities of the existing soft actuators in a variety of soft robotic applications including soft robotic grippers, soft planar robotic manipulators, quadrupedal soft crawling robots, and soft flipping robots.

Currently, the KiriSPA is without the ability to change its stiffness during the working procedures. The stiffness variable mechanism will be proposed and integrated with the KiriSPA in our future work, without affecting the multiple deformation behaviors of the KiriSPA, which further enhances the functionalities of SPAs.

Author Disclosure Statement

No competing financial interests exist.

Funding Information

This project is supported by the National Natural Science Foundation of China (Grant No. 52005036). This project is supported by the Beijing Institute of Technology Research Fund Program for Young Scholars and National Robotics Programme—Robotics Enabling Capabilities and Technologies (R-397-000-381-305).

Supplementary Material

Supplementary Data
Supplementary Figure S1
Supplementary Figure S2
Supplementary Figure S3
Supplementary Figure S4
Supplementary Table S1
Supplementary Movie S1
Supplementary Movie S2
Supplementary Movie S3
Supplementary Movie S4
Supplementary Movie S5

References

1. Laschi C, Mazzolai B, Cianchetti M. Soft robotics: technologies and systems pushing the boundaries of robot abilities. Sci Robot 2016;1:eaah3690.
2. Rus D, Tolley MT. Design, fabrication and control of soft robots. Nature 2015;521:467–475.
3. Sparrman B, Pasquier C du, Thomsen C, *et al.* Printed silicone pneumatic actuators for soft robotics. Addit Manuf 2021;40:101860.
4. Martinez RV, Glavan AC, Keplinger C, *et al.* Soft actuators and robots that are resistant to mechanical damage. Adv Funct Mater 2014;24:3003–3010.
5. Hawkes EW, Blumenschein LH, Greer JD, *et al.* A soft robot that navigates its environment through growth. Sci Robot 2017;2:eaan3028.
6. Katzschmann RK, DelPreto J, MacCurdy R, *et al.* Exploration of underwater life with an acoustically controlled soft robotic fish. Sci Robot 2018;3:eaar3449.
7. Guo J, Low JH, Liang X, *et al.* A hybrid soft robotic surgical gripper system for delicate nerve manipulation in digital nerve repair surgery. IEEE ASME Trans Mechatron 2019;24:1440–1451.
8. Cianchetti M, Ranzani T, Gerboni G, *et al.* Soft robotics technologies to address shortcomings in today's minimally invasive surgery: the STIFF-FLOP approach. Soft Robot 2014;1:122–131.
9. Agarwal G, Besuchet N, Audergon B, *et al.* Stretchable materials for robust soft actuators towards assistive wearable devices. Sci Rep 2016;6:34224.
10. Polygerinos P, Wang Z, Galloway KC, *et al.* Soft robotic glove for combined assistance and at-home rehabilitation. Robot Auton Syst 2015;73:135–143.
11. Wang Y, Yang X, Chen Y, *et al.* A biorobotic adhesive disc for underwater hitchhiking inspired by the remora suckerfish. Sci Robot 2017;2:eaan8072.
12. Lin HT, Leisk GG, Trimmer B. GoQBot: a caterpillar-inspired soft-bodied rolling robot. Bioinspir Biomim 2011; 6:026007.
13. Ilievski F, Mazzeo AD, Shepherd RF, *et al.* Soft robotics for chemists. Angew Chem 2011;50:1890–1895.
14. Hao Y, Gong Z, Xie Z, *et al.* A soft bionic gripper with variable effective length. J Bionic Eng 2018;15: 220–235.
15. Shepherd RF, Stokes AA, Freake J, *et al.* Using explosions to power a soft robot. Angew Chem 2013;52:2892–2896.
16. Joyee EB, Pan Y. A fully three-dimensional printed inchworm-inspired soft robot with magnetic actuation. Soft Robot 2019;6:333–345.
17. Wang H, Chen W, Yu X, *et al.* Visual servo control of cable-driven soft robotic manipulator. In: 2013 IEEE/RSJ International Conference on Intelligent Robots and Systems (IROS). Tokyo, Japan: IEEE; 2013, pp. 57–62.
18. Shepherd RF, Ilievski F, Choi W, *et al.* Multigait soft robot. Proc Natl Acad Sci U S A 2011;108:20400–20403.
19. Ranzani T, Cianchetti M, Gerboni G, *et al.* A soft modular manipulator for minimally invasive surgery: design and characterization of a single module. IEEE Trans Robot 2016;32:187–200.

20. Connolly F, Polygerinos P, Walsh CJ, *et al.* Mechanical programming of soft actuators by varying fiber angle. Soft Robot 2015;2:26–32.
21. Connolly F, Walsh CJ, Bertoldi K. Automatic design of fiber-reinforced soft actuators for trajectory matching. Proc Natl Acad Sci U S A 2017;114:51–56.
22. Sun Y, Yap HK, Liang X, *et al.* Stiffness customization and patterning for property modulation of silicone-based soft pneumatic actuators. Soft Robot 2017;4:251–260.
23. Mosadegh B, Polygerinos P, Keplinger C, *et al.* Pneumatic networks for soft robotics that actuate rapidly. Adv Funct Mater 2014;24:2163–2170.
24. Yap HK, Ng HY, Yeow CH. High-force soft printable pneumatics for soft robotic applications. Soft Robot 2016; 3:144–158.
25. Chen DH, Ushijima K. Prediction of the mechanical performance of McKibben artificial muscle actuator. Int J Mech Sci 2014;78:183–192.
26. Gorissen B, Volder MD, Greef AD, *et al.* Theoretical and experimental analysis of pneumatic balloon microactuators. Sens Actuator A Phys 2011;168:58–65.
27. Martinez RV, Fish CR, Chen X, *et al.* Elastomeric Origami: programmable paper-elastomer composites as pneumatic actuators. Adv Funct Mater 2012;22:1376–1384.
28. Tawk C, Panhuis MIH, Spinks GM, *et al.* Bioinspired 3D printable soft vacuum actuators for locomotion robots, grippers and artificial muscles. Soft Robot 2018;5:685–694.
29. Tawk C, Spinks GM, Panhuis MIH, *et al.* 3D printable linear soft vacuum actuators: their modeling, performance quantification and application in soft robotic systems. IEEE ASME Trans Mechatron 2019;24:2118–2129.
30. Jiao Z, Ji C, Zou J, *et al.* Vacuum-powered soft pneumatic twisting actuators to empower new capabilities for soft robots. Adv Mater Technol 2019;4:1800429.
31. Yang D, Verma MS, So JH, *et al.* Buckling pneumatic linear actuators inspired by muscle. Adv Mater Technol 2016;1:1600055.
32. Rogatinsky J, Gomatam K, Lim ZH, *et al.* A collapsible soft actuator facilitates performance in constrained environments. Adv Intell Syst 2022;2200085:2200085.
33. Nguyen PH, Zhang W. Design and computational modeling of fabric soft pneumatic actuators for wearable assistive devices. Sci Rep 2020;10:9638.
34. Moghadam AAA, Alaie S, Nath SD, *et al.* Laser cutting as a rapid method for fabricating thin soft pneumatic actuators and robots. Soft Robot 2018;5:443–451.
35. Low JH, Cheng N, Khin PM, *et al.* A bidirectional soft pneumatic fabric-based actuator for grasping applications. In: 2017 IEEE/RSJ International Conference on Intelligent Robots and Systems (IROS). Vancouver, Canada: IEEE; 2017, pp. 1180–1186.
36. Natividad R, del Rosario M, Chen CY, *et al.* A reconfigurable pneumatic bending actuator with replaceable inflation modules. Soft Robot 2018;5:304–317.
37. Lee H, Oh N, Rodrigue H. Expanding pouch patterns for programmable soft bending actuation. IEEE Robot Autom Mag 2020;27:65–74.
38. Yang HD, Asbeck AT. A layered manufacturing approach for soft and soft-rigid hybrid robots. Soft Robot 2020;7: 218–232.
39. Shyu TC, Damasceno PF, Dodd PM, *et al.* A Kirigami approach to engineering elasticity in nanocomposites through patterned defects. Nat Mater 2015;14: 785–789.
40. Rafsanjani A, Zhang Y, Liu B, *et al.* Kirigami skins make a simple soft actuator crawl. Sci Robot 2018;3:eaar7555.
41. Yamamoto Y, Harada S, Yamamoto D, *et al.* Printed multifunctional flexible device with an integrated motion sensor for health care monitoring. Sci Adv 2016;2:e1601473.
42. Tang Y, Lin G, Yang S, *et al.* Programmable Kiri-Kirigami metamaterials. Adv Mater 2017;29:1604262.
43. Blees MK, Barnard AW, Rose PA, *et al.* Graphene Kirigami. Nature 2015;524:204–207.
44. Lu X, Xu W, Li X. A soft robotic tongue-mechatronic design and surface reconstruction. IEEE ASME Trans Mechatron 2017;22:2102–2110.
45. Polygerinos P, Wang Z, Overvelde JTB, *et al.* Modeling of soft fiber-reinforced bending actuators. IEEE Trans Robot 2015;31:778–789.
46. Glick P, Suresh SA, Ruffatto D, *et al.* A soft robotic gripper with Gecko-inspired adhesive. IEEE Robot Autom Lett 2018;3:903–910.
47. Wei Y, Chen Y, Ren T, *et al.* A novel, variable stiffness robotic gripper based on integrated soft actuating and particle jamming. Soft Robot 2016;3:134–143.
48. Hao Y, Liu Z, Liu J, *et al.* A soft gripper with programmable effective length, tactile and curvature sensory feedback. Smart Mater Struct 2020;29:035006.
49. Liu S, Wang F, Liu Z, *et al.* A two-finger soft-robotic gripper with enveloping and pinching grasping modes. IEEE ASME Trans Mechatron 2021;26:146–155.
50. Deimel R, Brock O. A novel type of compliant and underactuated robotic hand for dexterous grasping. Int J Robot Res 2016;35:161–185.
51. Galloway KC, Becker KP, Phillips B, *et al.* Soft robotic grippers for biological sampling on deep reefs. Soft Robot 2016;3:23–33.
52. Bilodeau RA, White EL, Kramer RK. Monolithic fabrication of sensors and actuators in a soft robotic gripper. In: 2015 IEEE/RSJ International Conference on Intelligent Robots and Systems (IROS). Hamburg, Germany: IEEE; 2015, pp. 2324–2329.

Address correspondence to:
Jin Guo
School of Life Science
Beijing Institute of Technology
No. 5, South Street, Zhongguancun
Beijing 100081
China

E-mail: guojin0522@gmail.com